THE JOURNAL OF PHYSICAL CHEMISTRY B

ARTICLE

pubs.acs.org/JPCB

# Time-Dependent Current Distributions of a Two-Terminal Carbon Nanotube-Based Electronic Device

Shizheng Wen,[†,‡,§] SiuKong Koo,[†] ChiYung Yam,[*,†] Xiao Zheng,[*,§] YiJing Yan,[§] Zhongmin Su,[‡] Kangnian Fan,[∥] Li Cao,[⊥] Wenping Wang,[⊥] and GuanHua Chen[*,†]

[†]Department of Chemistry, Centre of Theoretical and Computational Physics, The University of Hong Kong, Hong Kong

[‡]Institute of Functional Material Chemistry, Faculty of Chemistry, Northeast Normal University, Changchun 130024, P. R. China

[§]Department of Chemistry, Hong Kong University of Science and Technology, Hong Kong

[∥]Shanghai Key Laboratory of Molecular Catalysis and Innovative Materials, Center for Theoretical Chemical Physics, Department of Chemistry, Fudan University, Shanghai, 200433, P. R. China

[⊥]Department of Computer Science, The University of Hong Kong, Hong Kong

**ABSTRACT:** We have performed time-dependent density-functional theory calculations to simulate the transient electrical response of a carbon nanotube-based electronic device. Time-dependent current density and electrostatic potential distribution are calculated and analyzed. Strong local vortices are observed for the current. In addition, the calculated dynamic admittance confirms that the dynamic response of the two-terminal device can be mapped onto the equivalent electric circuit reported in our previous work [Yam et al. *Nanotechnology* **2008**, *19*, 495203].

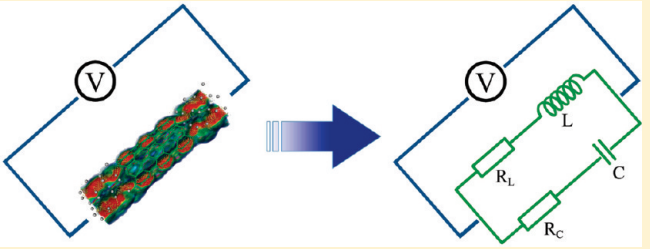


## I. INTRODUCTION

During the past few years there have been increasing interests in understanding time-dependent quantum transport through nanostructures. Both theoretical and experimental research efforts have been carried out.[1−13] There are two general approaches to treat the time-dependent quantum transport problem theoretically. One approach is to work in the frequency domain. For instance, Floquet theory has been applied to study electron transport under sinusoidal external voltage.[14−17] By considering all the frequencies and taking a Fourier transform of the results, the transient current response of the system can be recovered. Another approach is to work directly in the time domain and obtain the real-time current response of the system. However, until recently, most theoretical studies had been focused on simple model systems in which the electronic devices of primary interest are modeled by one- or few-level systems.[3] It is thus difficult to evaluate how the geometric and electronic structures of specific nanosized structures or materials would influence the transport process. Recently, time-dependent density-functional theory (TDDFT) formalisms have been developed.[7−12] A practical scheme has been proposed in order to simulate transient currents through realistic nanoscale devices.[7,10] In particular, dynamic current response of carbon nanotube (CNT)-based devices have been investigated.[18] The TDDFT formalism is based on an equation of motion (EOM) for the Kohn−Sham (KS) reduced single-electron density matrix which is equivalent to the well-known quantum kinetic equation. Alternatively, this formalism can be viewed as the first-principles Liouville−von Neumann equation.

In this manuscript, we generalize the TDDFT formalism[7] to calculate the current density distribution, and apply it to examine the transient current through a (8,0) CNT coupled to the left and right electrodes. In particular, we focus on analyzing the local current distribution. This paper is organized as follows: In section II, we outline our theoretical methodology and present the practical scheme for the evaluation of current density distribution. The simulation results are analyzed and discussed in section III. Finally, we conclude our findings in section IV.

## II. METHODOLOGY

Electron density function of any time-independent real physical system made of atoms and molecules is real analytic except at nuclei (a function is real analytic if it possesses derivatives of all orders and agrees with its Taylor series in a neighborhood of every point). This has been proved by Fournais et al. in 2004[19] and termed as time-independent holographic electron density theorem. Here, real analyticity or "holographic" property implies that any nonzero volume piece of ground-state electron density completely determines the electron density of the entire

**Special Issue:** Shaul Mukamel Festschrift

**Received:** November 20, 2010
**Revised:** February 9, 2011
**Published:** March 09, 2011

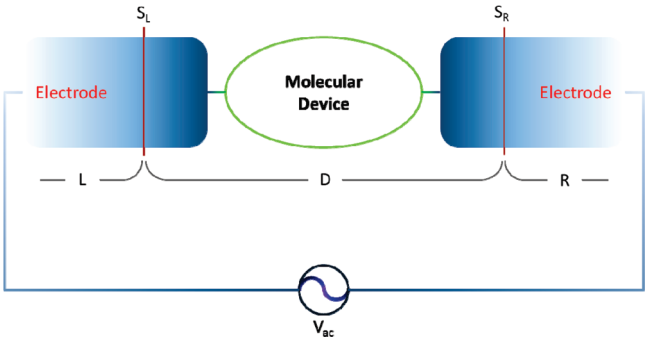


**Figure 1.** Schematic representation of the experimental setup for quantum transport through a molecular device. $L$, $R$, and $D$ denote the left electrode region, right electrode region and device region, respectively. $L$ and $R$ are connected to an external bias. $S_L(S_R)$ represents the interface between $D$ and $L(R)$. It should be noted that we include adequate part of the electrodes, i.e., shaded areas in the schematic diagram, into $D$, so that $S_L(S_R)$ will show bulk properties of $L(R)$.

system.[20] For time-dependent systems, there also exists a holographic time-dependent electron density theorem.[21] If the time-dependent external potential field on a finite physical system, $v(\vec{r},t)$, is real analytic in both $\vec{r}$ and $t$, and its electron density at a given time $t_0$, $\rho(\vec{r},t_0)$, is real analytic in $\vec{r}$ -space, then there is a one-to-one correspondence between $v(\vec{r},t)$ and the time-dependent electron density within any finite subspace $D$, $\rho_D(\vec{r},t)$.[7] As a result, $\rho_D(\vec{r},t)$ determines uniquely all the electronic properties of the entire time-dependent physical system. Therefore, the holographic time-dependent electron density theorem proves the existence of an exact density-functional theory for time-dependent open electronic systems. On the basis of the exact TDDFT for open systems, a practical first-principles approach has been developed to simulate transient electrical current through molecular devices.

The derivation of our TDDFT formalism for open systems starts from a closed EOM for the KS-reduced single-electron density matrix of the entire system, $\sigma(t)$:

$$i\dot{\sigma}(t) = [h(t), \sigma(t)] \tag{1}$$

where $h(t)$ is the KS Fock matrix. Figure 1 illustrates a simple open system schematically. By using atomic orbital basis sets to expand the density matrix, we can partition $\sigma$ as

$$\sigma = \begin{bmatrix} \sigma_L & \sigma_{LD} & \sigma_{LR} \\ \sigma_{DL} & \sigma_D & \sigma_{DR} \\ \sigma_{RL} & \sigma_{RD} & \sigma_R \end{bmatrix} \tag{2}$$

where $\sigma_L$, $\sigma_D$, and $\sigma_R$ are the diagonal blocks corresponding to the left electrode $L$, the device region $D$, and the right electrode $R$, respectively; $\sigma_{DL}$ is the off-diagonal block between $D$ and $L$, and $\sigma_{RL}$, $\sigma_{LD}$, $\sigma_{RD}$, $\sigma_{LR}$, and $\sigma_{DR}$ have similar definitions. We can also partition the KS Fock matrix $h$ in the same manner. Thus, we can get the EOM for $\sigma_D$:

$$\begin{aligned} i\dot{\sigma}_D &= [h_D, \sigma_D] + \sum_{\alpha=L,R} (h_{D\alpha}\sigma_{\alpha D} - \sigma_{D\alpha}h_{\alpha D}) \\ &= [h_D, \sigma_D] - i\sum_{\alpha=L,R} Q_\alpha \end{aligned} \tag{3}$$

where $Q_L$ and $Q_R$ are the dissipative terms due to $L$ and $R$, respectively. According to the holographic time-dependent electron density theorem, $Q_\alpha$ is in principle a functional of the electron density in the reduced system $D$, $\rho_D(\vec{r},t)$. Transforming $\rho_D$ into $\sigma_D$, a formally closed form of eq 3 can be recast as follows:

$$\begin{aligned} i\dot{\sigma}_D &= [h_D[\vec{r},t;\sigma_D(\vec{r},t)], \sigma_D(\vec{r},t)] \\ &\quad - i\sum_{\alpha=L,R} Q_\alpha[\vec{r},t;\sigma_D(\vec{r},t)] \end{aligned} \tag{4}$$

Employing the Keldysh nonequilibrium Green's function (NEGF) formalism, we have

$$\begin{aligned} Q_\alpha(t) = -\sum \int_{-\infty}^{+\infty} d\tau [G^<(t,\tau)\Sigma_\alpha^a(\tau,t) + G^a(t,\tau)\Sigma_\alpha^<(\tau,t) \\ + H.c.] \end{aligned} \tag{5}$$

where $G^<$ and $G^a$ are the lesser and advanced Green's functions respectively, and $\Sigma^<$ and $\Sigma^a$ are the lesser and advanced self-energies, respectively. In the practical numerical calculation of $Q_\alpha$, the adiabatic wide-band limit (AWBL) approximation[3,7,22] is adopted, where the bandwidths of both electrodes are assumed to be infinitely large and the self-energy $\Sigma_\alpha$ is treated as energy independent. The time-dependent electric current through electrode $\alpha$ ($\alpha = L$ or $R$) can be calculated as

$$I_\alpha(t) = -Tr[Q_\alpha(t)] \tag{6}$$

The transient dynamics of the device $D$ is solved by directly integrating eq 4 subjected to the potential boundary conditions at the left and right interfaces of the simulation box.

The reduced single-electron density matrix $\sigma_D(t)$ can be partitioned into two parts: $\sigma_D^{(0)}$ and $\delta\sigma_D(t)$, where $\delta\sigma_D(t)$ is the induced electron density matrix by the external field.[23,24] We have

$$\delta\rho(\vec{r},t) = \sum_{\mu,\nu\in D} \delta\sigma_{\mu\nu}(t)\chi_\nu^*(\vec{r})\chi_\mu(\vec{r}) \tag{7}$$

where $\delta\rho(\vec{r},t)$ is the induced electron density, and $\chi_\mu(\chi_\nu)$ is the $\mu(\nu)$th atomic basis function.

The current density operator is $\hat{\vec{j}}(\vec{r}) = (2i)^{-1}\Sigma_s\{[\nabla\hat{\psi}_s^\dagger(\vec{r})]\hat{\psi}_s(\vec{r}) - \hat{\psi}_s^\dagger(\vec{r})\nabla\hat{\psi}_s(\vec{r})\}$, where $\hat{\psi}_s^\dagger(\hat{\psi}_s)$ is the creation (annihilation) operator for an electron occupying molecular orbital $\psi_s$. Similarly, spanned by an atomic basis set $\{\chi_\nu\}$, the induced current density $\vec{j}(\vec{r},t)$ is expressed by,

$$\begin{aligned} \vec{j}(\vec{r},t) = (2i)^{-1}\sum_{\mu,\nu\in D} \delta\sigma_{\mu\nu}(t)[\chi_\mu(\vec{r})\nabla\chi_\nu^*(\vec{r}) \\ - \chi_\nu^*(\vec{r})\nabla\chi_\mu(\vec{r})] \end{aligned} \tag{8}$$

Usually $\chi_\mu(\vec{r})$ is a real function, and hence $\chi_\mu^*(\vec{r}) = \chi_\mu(\vec{r})$, we have

$$\vec{j}(\vec{r},t) = -\sum_{\mu\nu} \mathrm{Im}[\delta\sigma_{\mu\nu}(t)]\chi_\mu(\vec{r})\nabla\chi_\nu(\vec{r}) \tag{9}$$

Therefore, $\vec{j}(\vec{r},t)$ is only determined by the imaginary part of $\delta\sigma_D(t)$. In principle, only the longitudinal component of the current density can be obtained by TDDFT calculation, i.e., the longitudinal current density has real physical meaning while the transverse component does not. However, in practice, it has been argued that KS current density $\vec{j}(\vec{r},t)$ is a good approximation to exact value for both longitudinal and transverse components.[25] It should be noted that the magnetic field is neglected in TDDFT.[26,27] It can be included in time-dependent current density functional theory (TDCDFT).[28−30] Di Ventra et al. have developed a TDCDFT method for open systems via real-time propagation of a stochastic Schrödinger equation.[29] Yuen-Zhou et al. have proposed


dx.doi.org/10.1021/jp1110949 |J. Phys. Chem. B 2011, 115, 5519–5525

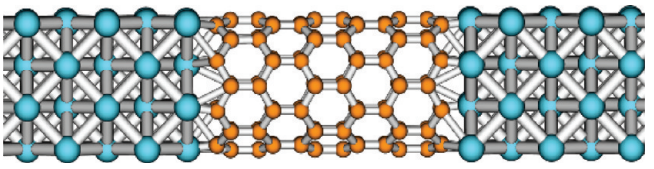

**Figure 2.** The ball and stick representation of our Al−CNT−Al system. The CNT is connected to the Al(100) surface. The system consists of 96 C atoms and 48 Al atoms in each leads.

a TDCDFT KS scheme for an open system.[30] Di Ventra et al.[27] have also found that the current density calculated by TDDFT with the adiabatic local density approximation (ALDA) for exchange-correlation (XC) functional are qualitatively similar to that obtained by TDCDFT with the Vignale−Kohn XC functional.[28] However, it should be emphasized that this qualitative similarity is true only under small bias voltages when the viscosity of the electron liquid is not large.[27]

In our calculations, the crystal structure of aluminum is adopted for the electrodes, and the CNT segment is extracted from an ideal infinitely long tube. As shown in Figure 2, both ends of the CNT are connected to the Al(100) surface with a preset separation of 1.5 Å, which is welded to the electrodes covalently.[31] We include explicitly in the simulation box 32 Al atoms in each electrode, together with 96 C atoms of the CNT. The ground-state KS Fock matrix of the extended system (including extra portions of leads of 16 atoms on each side) is calculated self-consistently with LDA. Since the aluminum metal is a good conductor, the induced electrostatic potential by external voltage is constant for the bulk electrode far away from the device. In our calculations, the constant-induced electrostatic potential provides the boundary condition for solving the Poisson equation for Hartree potential inside the simulation box. The same procedure has been widely adopted in the simulation of quantum transport.[9,22] All calculations are carried out with our in-house built software package LODESTAR.[23,24,32,33] The minimal basis set STO-3G is adopted.

## III. RESULTS AND DISCUSSION

**A. Transient Current Density and Potential.** With the above approach, we study how the current flows through the device by calculating the current density at different times. In Figure 3a−c, we plot three snapshots of the current density of the system at time $t$ = 0.4, 4, and 20 fs after the switch-on of voltage to illustrate the current evolution. In the Figures, we use the cones to represent the local current density vectors in the middle plane, and plot the local current intensity in the lower half of the simulation box, where the color varies from blue to red representing the increasing magnitude of current density. The vortex-like structures are clearly observed for the current.

In the simulation, the bias voltage is turned on exponentially, $V(t) = V_0(1 - e^{-t/a})$ with $V_0$ = 0.1 mV and time constant $a$ = 1 fs. We applied this time-dependent voltage on the right electrode, while keeping the left electrode at 0 V at all times, so that there is a time-dependent voltage difference across the device. At $t$ = 4 fs, the voltage reaches nearly its maximum as shown in Figure 4a. This can also be confirmed by analyzing the spatial distribution of the potential as shown in Figure 5b,c, where the potentials at $t$ = 4 and 20 fs are similar. In the meantime, the transient current is 6.3 and 10.9 nA at $t$ = 4 and 20 fs, respectively. The currents are quite

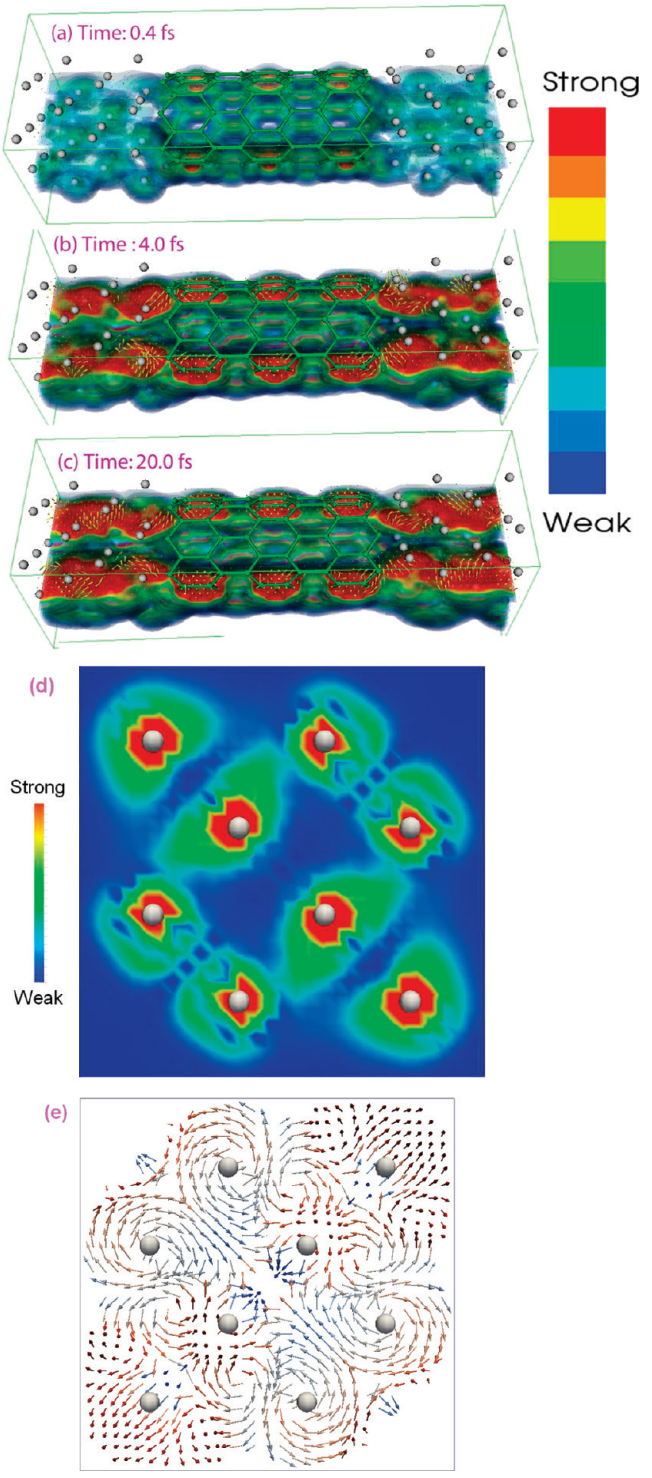


**Figure 3.** Panels a, b, and c show the local current density distribution at $t$ = 0.4 fs, $t$ = 4 fs, and $t$ = 20 fs, respectively. In the figures, gray spheres represent aluminum atoms, and the green balls and sticks represent the CNT. The cones represent the on-site current density vectors, and the color ranging from blue to red represents the increasing intensity of current density. For clarity we only plot the bottom half of the device region. (d) Magnitude of $\nabla \times j(\vec{r})$ of a plane cutting through aluminum atoms at $t$ = 20 fs. (e) Direction of current density on the same plane as in panel d. Local vortices are clearly observed.

different at the two instants; while the patterns of the corresponding local current distributions are similar. This is interesting, as it


dx.doi.org/10.1021/jp1110949 |J. Phys. Chem. B 2011, 115, 5519–5525

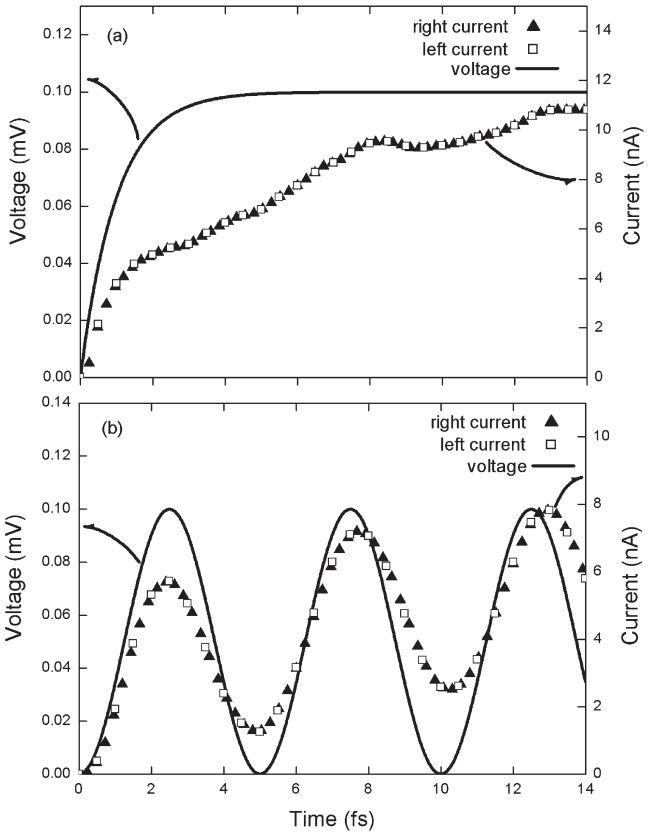


**Figure 4.** (a,b) Transient current (solid triangles and open squares) and applied bias voltage (solid lines) for the Al−CNT−Al system. (a) The bias voltage is turned on exponentially, $V_0(1 - e^{-t/a})$ with $V_0 = 0.1$ mV and time constant $a = 1$ fs. (b) The bias voltage is sinusoidal with a period of 5 fs. The solid triangles are representing current from the right electrode, and the open squares are current from the left electrode.

indicates that, despite the difference in overall intensity, the spatial distribution can be similar.

To describe the observed behavior of transient current through the device, we calculated $\nabla \times \vec{j}(\vec{r})$ to analyze the local current distribution. It is observed that, in addition to the overall direction of the current, the current density shows strong local characteristics. We have plotted $|\nabla \times \vec{j}(\vec{r})|$ for a plane around aluminum atoms in Figure 3d. We observe that $\nabla \times \vec{j}(\vec{r})$ is strong around the atoms. As shown in Figure 3e, local currents are characterized by the hydrodynamic features as others reported.[34] We note that the vortices mostly concentrate around the atoms, especially near the aluminum atoms, which is in agreement with our analysis for $|\nabla \times \vec{j}(\vec{r})|$ as shown in Figure 3d. We also looked into the direction of the "curl vectors" in the vortices, which basically representing the direction of the vortex axis, and found that the directions of the vertices are actually quite random, despite there being a net transport direction of the current.

Furthermore, we calculated the total current flows through any surfaces within the device, and confirmed that the total current obtained from integration of current density is consistent with that calculated via eq 6. For example, at $t = 14$ fs, for the middle plane, which is normal to the axis of the CNT, the integration of current density of that surface gives 10.6 nA, while the current calculated at the electrode is 10.8 nA. The difference can be attributed to the contributions due to the couplings between the electrodes and the device.

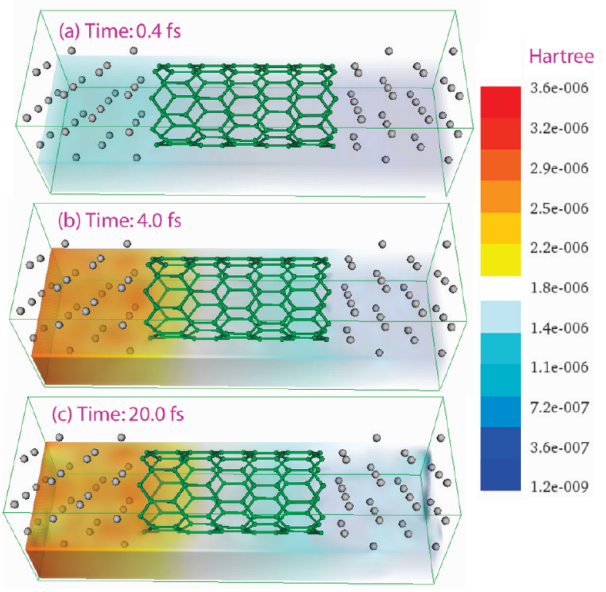


**Figure 5.** Panels a, b, and c show the spatial distribution of electrostatic potential at time 0.4, 4.0, and 20.0 fs, respectively. The system is under the exponentially turned on bias voltage $V_0(1 - e^{-t/a})$ with $V_0 = 0.1$ mV and decay time constant $a = 1$ fs. For clarity we show only the bottom half of the device region.

**B. Transient Current and Dynamic Admittance.** Figures 4a, b shows the current versus time for two different types of bias voltage switched on at $t = 0$. In Figure 4a, the bias voltage $V_b$ is turned on exponentially. We observed that the relaxation time, i.e., the time needed by the system to reach the final steady state, is about 14 fs. As discussed before,[18,35] such a fast process is due to the fact that the transient dynamics involves electrons only. We have also simulated the current response under a sinusoidal applied voltage, which had been widely used in the Floquet theory approach,[14−17] as shown in Figure 4b. The sinusoidal voltage takes the form of $V(t) = V_0/2[1 - \cos(2\pi t/a)]$, with $V_0 = 0.1$ mV and oscillation period $a = 5$ fs. The external voltage is applied only on the right electrode, while the left electrode is voltage-free at all times. After the bias voltage is switched on, sinusoidal current response is observed, as expected. A phase delay is observed in the current response to bias voltage, which implies that the device is overall inductive at this frequency. In addition, the current was building up its shape gradually in the first few cycles, and eventually become quasi-steady, oscillating between 2.5 nA and 9.0 nA. We also performed simulation with a different initial state. Starting with the system initially in the steady state established at bias voltage 0.1 mV, we applied the same sinusoidal voltage to the system, i.e., the bias voltage is turned off from 0.1 mV in the first 2.5 fs and turned on and off at a period of 5 fs afterward. Inspection of the current versus time plot (not shown here) shows that the same final quasi-steady state is reached. This shows that the initial state memory is washed out at long time limit. To investigate the potential to be used as elements in a memristive system.[36−38] We have plotted a transient current−voltage ($I$−$V$) curve in Figure 6. The first cycle gives a cross in the $I$−$V$ curve. Then the $I$−$V$ curve became a half ellipse in the second cycle, followed by a series of ellipses in the later cycles. This shows that there is a constant phase difference between the current and the applied voltage after the system reached a quasi-steady state. Clearly, the system behaves classically in this case,


dx.doi.org/10.1021/jp1110949 |J. Phys. Chem. B 2011, 115, 5519–5525

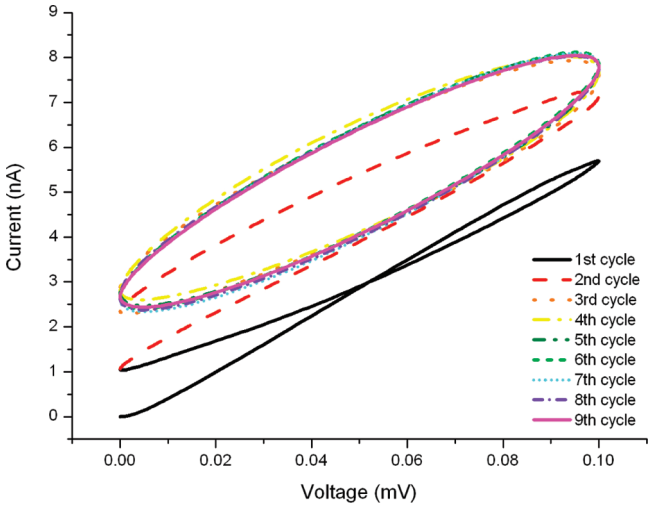


**Figure 6.** The transient current−voltage (I−V) curve for the studied system under a time-dependent sinusoidal voltage applied to the right electrode only, $V(t) = V_0/2[1 - \cos(2\pi t/a)]$, with $V_0 = 0.1$ mV and oscillation period $a = 5$ fs. Nine complete cycles are plotted in the graph, and each cycle is represented with a different line type.

and memristive effects were not observed when the quasi-steady oscillatory current is established. We believe those interesting memristive phenomena will be captured by simulations of nonlinear response, but may not be in the present case. An extensive study on the memristive property beyond the linear response regime would be of interest.

It is observed that the currents entering the system are exactly the same in magnitude as the current leaving. This is because the system has central inversion symmetry, and there is thus no transient charge accumulation or depletion inside the device. This is further confirmed by analyzing the potential distribution, and the charge distributions. Due to symmetry, the admittance matrix element $G_{\alpha\beta}(\omega)(\alpha,\beta = \mathrm{L,R})$ satisfies $G_{LL} = G_{RR} = -G_{LR} = -G_{RL} = G(\omega)$.[39−41] We obtain the dynamic admittance by $G(\omega) = I(\omega)/V(\omega)$. We have verified that our calculations are in the linear response regime. The nonlinear response is more complex, and it has been discussed for the model system elsewhere.[35] Figure 7a shows the real and imaginary parts of the resulting dynamic admittance. It is obvious that, in the linear response regime, the dynamic admittance for different types of bias voltage should be the same for the same system. This is confirmed by our numerical results for both exponential and sinusoidal time-dependent bias voltages as shown in Figure 7a.

**C. Equivalent Circuit.** According to the above results and analysis,[18,35] our device can be modeled by the classical circuit depicted in Figure 7b. At zero frequency, the steady state current goes only through the $R-L$ branch. $R_L$ is simply the steady state resistance,[41,42] which is calculated to be 10.17 kΩ. The charge relaxation resistance $R_C = h/4e^2$ is independent of the transmission details.[43] At a high frequency, the dynamic response is capacitor-like and voltage lags current.[44] The current enters into the device region from the left electrode, a part of it, $I_C$, charges the left interface.[11] The remaining current, $I_L$, goes straight through the device and is joined by $I_C$ at the right interface. Under an AC bias voltage of frequency $\omega$, its dynamic admittance can be expressed as $G(\omega) = (R_C + 1/-i\omega C)^{-1} + (R_L + i\omega L)^{-1}$. The values of $L$ and $C$ are calculated via fitting the calculated dynamic admittance based on the above formula. The resulting

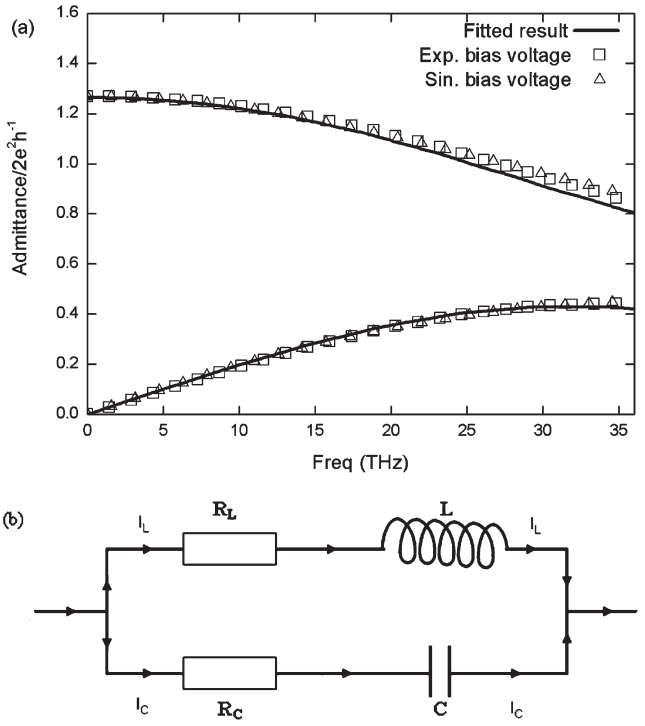


**Figure 7.** (a) Dynamic admittance calculated with an exponential bias voltage (open squares) turned on at $t = 0$ and a sinusoidal bias voltage (open triangles) turned on at $t = 0$. The solid lines show the results fitted to the classical circuit. The upper curves are the real part of the admittance, while the lower ones are the imaginary part. (b) The equivalent electric circuit of our system. The fitted values of each component are as follows: $L = 31.1$ pH, $R_L = 10.17$ kΩ, $C = 0.049$ aF, and $R_C = 6.45$ kΩ.

values of $L$ and $C$ are 31.1 pH and 0.049 aF, respectively. As the bias voltage is turned on, induced charge starts to accumulate at the two interfaces, with a characteristic charging time, $\tau_C = R_C C = 0.32$ fs, for the $R-C$ branch. The capacitance can also be estimated directly from the excess charge at the interface via $C = Q/V_b$.[18] The kinetic inductance $L$ is determined by the dwell time $\tau_d$ of the electrons inside the device as $L \sim \tau_d h/e^2$, where $\tau_d \sim l/v_f$.[44] From the results, our device has very small values of $L$ and $C$, leading to the short switching time for this nanoscale device discussed. By analyzing the equivalent circuit, we can calculate the response of the current. For an exponential bias voltage, i.e., $V(t) = V_0(1 - e^{-t/a})$, the current going through the circuit would be

$$I(t) = \frac{V_0[L - e^{-R_L t/L}L + aR_L(e^{-t/a} - 1)]}{R_L(L - aR_L)} + \frac{V_0 C}{a - CR_C}(e^{-t/a} - e^{-t/cR_C}) \quad (10)$$

When $a$ tends to zero, the bias voltage reduced to a step-function, and the current can be express as $I(t) = (V_0/R_L)(1 - e^{-R_L t/L}) + (V_0/R_C)(e^{-t/cR_C})$. In this case, the current is composed of two simple components, which are the current going through the $R-L$ and $R-C$ arm of the circuit. The current going through the $R-L$ arm exponentially increases with the ratio between $R_L$ and $L$ as the time constant, i.e., $R_L/L$; this part of the current simply increases with time with the effect of the inductor. On the other hand, the current going through the $R-C$ arm exponentially


dx.doi.org/10.1021/jp1110949 |J. Phys. Chem. B 2011, 115, 5519–5525

decreases with the time constant inversely proportional to $R_C$ and $C$, i.e., $1/R_CC$, as the capacitor is charging up, and hence this part of the current decreases with time. Therefore, the total current will first drop and then increase, and eventually become steady.

## IV. CONCLUDING REMARKS

Our first-principles simulation includes all electrons and full atomistic details for both the electrodes and the nanoscopic device. In our previous work, we carried out first-principles simulation of a (5,5) CNT-based device, and found that the dynamic electric response of a two-terminal coherent conductor can be mapped precisely onto an equivalent classical electrical circuit. In this work, we study instead a (8,0) CNT, re-examine its dynamic electric response, and thus reconfirm our early finding on the equivalent electric circuit. The potential of displaying memristive properties is noted in the studied electronic device. This is a very interesting issue, as it may open new frontiers in nanoelectronics. Further investigations, are desirable, especially for calculations in nonlinear response regime. The distributions of local current density and electrostatic potential in space are examined and analyzed at every time step. Large local current density vortices are observed as the current flow is established. We find similar spatial distributions of the current for different overall current intensities. Detailed temporal evolution and spatial distribution of current and electrostatic potential provide intuitive pictures of the underlying microscopic processes inside the nanoelectronic devices and thus yield important guidelines for designing such devices in future.

## AUTHOR INFORMATION

### Corresponding Author

*E-mail: yamcy@yangtze.hku.hk (C.Y.); xzheng@yangtze.hku.hk (X.Z.); ghc@everest.hku.hk (G.C.).

## ACKNOWLEDGMENT

The authors thank Thomas Frauenheim, Bill Goddard, and Thomas Niehaus for stimulating discussions. Support from the Hong Kong Research Grant Council (HKU 7011/06P, 7013/07P, 7008/08P, HKUST 9/CRF/08, and N_HKU 764/05), the University Grant Council (AoE/P-04/08), and the National Science Foundation of China (NSFC 20828003) is also acknowledged.

## REFERENCES

(1) Gabelli, J.; Fève, G.; Berroir, J.-M.; Placais, B.; Cavanna, A.; Etienne, B.; Jin, Y.; Glattli, D. C. *Science* **2006**, *313*, 499–502.

(2) Prêtre, A.; Thomas, H.; Büttiker, M. *Phys. Rev. B* **1996**, *54* 8130–8143.

(3) Maciejko, J.; Wang, J.; Guo, H. *Phys. Rev. B* **2006**, *74*, 085324.

(4) Topinka, M. A.; LeRoy, B. J.; Shaw, S. E. J.; Heller, E. J.; Westervelt, R. M.; Maranowski, K. D.; Gossard, A. C. *Science* **2000**, *289*, 2323–2326.

(5) Ke, S. H.; Liu, R.; Yang, W. T.; Baranger, H. U. *J. Chem. Phys.* **2010**, *132*, 234105.

(6) Zheng X.; Chen, G. H. arXiv:physics/0502021.

(7) Zheng, X.; Wang, F.; Yam, C. Y.; Mo, Y.; Chen, G. H. *Phys. Rev. B* **2007**, *75*, 195127.

(8) (a) Stefanucci, G.; Almbladh, C.-O. *Europhys. Lett.* **2004**, *67*, 14–20. (b) Stefanucci, G.; Almbladh, C.-O. *Phys. Rev. B* **2004**, *69*, 195318. (c) Stefanucci, G.; Perfetto, E.; Cini, M. *Phys. Rev. B* **2010**, *81*, 115446.

(9) Kurth, S.; Stefanucci, G.; Almbladh, C.-O.; Rubio, A.; Gross, E. K. U. *Phys. Rev. B* **2005**, *72*, 035308.

(10) Zheng, X.; Chen, G. H.; Mo, Y.; Koo, S. K.; Tian, H.; Yam, C. Y.; Yan, Y. J. *J. Chem. Phys.* **2010**, *133*, 114101.

(11) Yuen-Zhou, J.; Tempel, D. G.; Rodríguez-Rosario, C. A.; Aspuru-Guzik, A. *Phys. Rev. Lett.* **2010**, *104*, 043001.

(12) Tempel, D. G.; Watson, M. A.; Olivares-Amaya, R.; Aspuru-Guzik, A. arXiv:1004.0189v2.

(13) Myöhänen, P.; Stan, A.; Stefanucci, G.; van Leeuwen, R. *Phys. Rev. B* **2009**, *80*, 115107.

(14) (a) Tikhonov, A.; Coalson, R. D.; Dahnovsky, Y. *J. Chem. Phys.* **2002**, *116*, 10909–10920. (b) Tikhonov, A.; Coalson, R. D.; Dahnovsky, Y. *J. Chem. Phys.* **2002**, *117*, 567–580.

(15) Dahnovsky, Y. *Phys. Rev. B* **2009**, *80*, 165305.

(16) Stafford, C. A.; Wingreen, N. S. *Phys. Rev. Lett.* **1996**, *76* 1916–1919.

(17) (a) Creffield, C. E; Platero, G. *Phys. Rev. B* **2002**, *65*, 113304. (b) Creffield, C. E; Platero, G. *Phys. Rev. B* **2002**, *66*, 235303. (c) Brandes, T.; Aguado, R.; Platero, G. *Phys. Rev. B* **2004**, *69*, 205326.

(18) Yam, C. Y.; Mo, Y.; Wang, F.; Li, X. B.; Chen, G. H.; Zheng, X.; Matsuda, Y.; Kheli-Tahir, J.; Goddard, W. A., III. *Nanotechnology* **2008**, *19*, 495203.

(19) (a) Fournais, S.; Hoffmann-Ostenhof, M.; Hoffmann-Ostenhof, T. *Commun. Math. Phys.* **2002**, *228*, 401–415. (b) Fournais, S.; Hoffmann-Ostenhof, M.; Hoffmann-Ostenhof, T.; Sørensen, T. Ø. *Ark. Mat.* **2004**, *42*, 87–106.

(20) Riess, J.; Münch, W. *Theor. Chim. Acta* **1981**, *58*, 295–300.

(21) (a) Zheng, X.; Wang, F.; Chen, G. H. arXiv:quant-ph/0606169. (b) Yam, C. Y.; Zheng, X.; Chen, G. H. *J. Comput. Theor. Nanosci.* **2006**, *3*, 857–863. (c) Chen, G. H. In *Recent Progress in Computational Sciences and Engineering*; Simos, T.; Maroulis, G., Eds.; Lecture Series on Computer and Computational Sciences; Brill: Leiden, 2006; Vol. 7, p 803.

(22) Jauho, A.-P.; Wingreen, N. S.; Meir, Y. *Phys. Rev. B* **1994**, *50* 5528–5544.

(23) (a) Yokojima, S.; Chen, G. H. *Chem. Phys. Lett.* **1998**, *292*, 379–383. (b) Yokojima, S.; Chen, G. H. *Phys. Rev. B* **1999**, *59*, 7259–7262.

(24) (a) Yam, C. Y.; Yokojima, S.; Chen, G. H. *J. Chem. Phys.* **2003**, *119*, 8794–8803. (b) Yam, C. Y.; Yokojima, S.; Chen, G. H. *Phys. Rev. B* **2003**, *68*, 153105. (c) Wang, F.; Yam, C. Y.; Chen, G. H. *J. Chem. Phys.* **2007**, *126*, 134104.

(25) D'Agosta, R.; Vignale, G. *Phys. Rev. B* **2005**, *71*, 245103.

(26) Moldoveanu, V.; Manolescu, A.; Gudmundsson, V. *New J. Phys.* **2009**, *11*, 073019.

(27) Sai, N.; Bushong, N.; Hatcher, R.; Ventra, M. Di *Phys. Rev. B* **2007**, *75*, 115410.

(28) Vignale, G.; Kohn, W. *Phys. Rev. Lett.* **2006**, *77*, 2037–2040.

(29) (a) Di Ventra, M.; D'Agosta, R. *Phys. Rev. Lett.* **2007**, *98*, 226403. (b) D'Agosta, R.; Di Ventra, M. *Phys. Rev. B* **2008**, *78*, 165105.

(30) Yuen-Zhou, J.; Rodríguez-Rosario, C. A.; Aspuru-Guzik, A. *Phys. Chem. Chem. Phys.* **2009**, *11*, 4509–4522.

(31) Varga, K.; Pantelides, S. T. *Phys. Rev. Lett.* **2007**, *98*, 076804.

(32) Chen, G. H.; Yam, C. Y.; Yokojima, S.; Liang, W. Z.; Wang, X. J.; Wang, F.; Zheng, X. "Software". Homepage of GuanHua Chen Group. Accessed on November 2010. http://yangtze.hku.hk/new/software.php.

(33) (a) Liang, W. Z.; Yokojima, S.; Chen, G. H. *J. Chem. Phys.* **1999**, *110*, 1844–1855. (b) Liang, W. Z.; Yokojima, S.; Zhou, D. H.; Chen, G. H. *J. Phys. Chem. A* **2000**, *104*, 2445–2453. (c) Liang, W. Z.; Wang, X. J.; Yokojima, S.; Chen, G. H. *J. Am. Chem. Soc.* **2000**, *122*, 11129–11137. (d) Liang, W. Z.; Yokojima, S.; Ng, M. F.; Chen, G. H.; He, G. *J. Am. Chem. Soc.* **2001**, *123*, 9830–9836.

(34) D'Agosta, R.; Di Ventra, M. *J. Phys.: Condens. Matter* **2006**, *18*, 11059–11065.

(35) Mo, Y.; Zheng, X.; Chen, G. H.; Yan, Y. J. *J. Phys.: Condens. Matter* **2009**, *21*, 355301.
(36) (a) Chua, L. O. *IEEE Trans. Circuit Theory* **1971**, *18*, 507. (b) Chua, L. O.; Kang, S. M. *Proc. IEEE* **1976**, *64*, 209.
(37) Strukov, D. B.; Snider, G. S.; Stewart, D. R.; Williams, R. S. *Nature* **2008**, *453*, 80.
(38) Di Ventra, M.; Pershin, Y. V.; Chua, L. O. *Proc. IEEE* **2009**, *7*, 1717–1724.
(39) Wang, B.; Wang, J.; Guo, H. *Phys. Rev. Lett.* **1999**, *82*, 398–401.
(40) (a) Fu, Y.; Dudley, S. C. *Phys. Rev. Lett.* **1993**, *70*, 65–68. (b) Fu, Y.; Dudley, S. C. *Phys. Rev. Lett.* **1993**, *71*, 466–466.
(41) (a) Landauer, R. *IBM J. Res. Dev.* **1957**, *1*, 223–231. (b) Landauer, R. *Philos. Mag.* **1970**, *21*, 863–867.
(42) (a) Büttiker, M.; Imry, Y. *J. Phys. C: Solid State Phys.* **1985**, *18*, L467–L472. (b) Büttiker, M.; Imry, Y.; Landauer, R.; Pinhas, S. *Phys. Rev. B* **1985**, *31*, 6207–6215.
(43) (a) Büttiker, M.; Prêtre, A.; Thomas, H. *Phys. Rev. Lett.* **1993**, *70*, 4114–4117. (b) Büttiker, M.; Prêtre, A.; Thomas, H. *Phys. Rev. Lett.* **1993**, *71*, 465–465.
(44) Wang, J.; Wang, B. G.; Guo, H. *Phys. Rev. B* **2007**, *75*, 155336.